

GIANT MAGNETO-IMPEDANCE AND ITS APPLICATIONS

C. Tannous and J. Gieraltowski

Laboratoire de Magnétisme de Bretagne,

CNRS UMR-6135, Université de Bretagne Occidentale,

BP: 809 Brest CEDEX, 29285 FRANCE,

Tel.: (33) 2.98.01.62.28, FAX:(33) 2.98.01.73.95 E-mail: tannous@univ-brest.fr

Abstract

The status of Giant Magneto-Impedance effect is reviewed in wires, ribbons and multilayered soft ferromagnetic thin films. After establishing the theoretical framework for the description of the effect, and the constraints any material should have in order to show the effect, experimental work in wires, ribbons and multilayered thin films is described. Existing and potential applications of the effect in electronics and sensing are highlighted.

PACS numbers: 75.70.-i, 75.70.Ak, 85.70.Kh, 07.55.Ge

Keywords: Magnetic Materials. Transport. Magneto-impedance. Sensors. Wires. Thin films.

I. INTRODUCTION

Magnetoimpedance (MI) consists of a change of total impedance of a magnetic conductor (usually ferromagnetic) under application of a static magnetic field H_{dc} . When an ac current, $I = I_0 e^{j\omega t}$ of magnitude I_0 and angular frequency $\omega (= 2\pi f$, with f the ordinary frequency) flows through the material, it generates, by Ampère's Law, a transverse magnetic field inducing some magnetization. At low frequency, the change in the transverse magnetization generates an additional inductive voltage V_L across the conductor: $V = RI + V_L$ where R is the resistance. Hence MI can be written as $Z = R + j\omega\phi/I$, where the imaginary part is given by the ratio of magnetic flux to ac current and MI field dependence is related to the transverse permeability. When frequency increases the current gets distributed near the surface of the conductor, changing both resistive and inductive components of the total voltage V . The field dependence of MI is dictated by skin depth $\delta_s = \frac{c}{\sqrt{2\pi\omega\sigma\mu}}$ where c is the velocity of light, σ the conductivity and μ the permeability (For non magnetic ordinary metals, $\mu = 1$). The current distribution is governed not only by the shape of the conductor and frequency but also the transverse magnetization depending on H_{dc} .

Typically MI increases with frequency, attains a maximum at frequencies for which the skin effect is strong ($\delta_s \ll a$ where a is a characteristic length scale such as the wire radius or ribbon/film thickness) and then decreases since permeability becomes insensitive to the field at high enough frequency.

MI effect is ordinarily weak and did not attract much attention in the past. Interest in MI was triggered in the early 90's when Panina et al. [1] and Beach et al. [2] reported a very large (Giant) MI effect in amorphous ferromagnetic FeCoSiB wires with small magnetic fields and at relatively low frequencies (see Fig. 1). This shows that a large variation of the MI is observable in a finite frequency range for reasons that will be explained in later sections. Later on, Machado et al. [3] observed a smaller effect in $\text{Fe}_{4.6}\text{Co}_{70.4}\text{Si}_{15}\text{B}_{15}$ thin films and Beach et al. [4] in ribbons.

The dramatic variation of the MI (that can reach in some cases values larger than 800%) with small magnetic fields (a few Oersteds) and at relatively low frequencies (tens of MHz) in widely available materials is the origin of the interest in the Giant MagnetoImpedance (GMI) effect.

GMI materials share the property of being magnetically soft (easy to magnetize) and are now available as wires (typical diameter of the order of a mm), microwires (typical diameter of the order of a micron), ribbons, magnetically coated metallic (usually nonmagnetic) wires (tubes), thin films and multilayers, albeit, the effect itself occurs with widely differing magnitude depending on the geometry, the constituent materials and their layering.

In order to clearly identify GMI, several observations should be made:

1. A very large change (of the order of at least 100% variation) of the impedance should occur with an external dc magnetic field H_{dc} . The change expressed in % is defined by the largest value of the ratio:

$$r(H_{dc}) = 100 \times |Z(H_{dc}) - Z(H_{sat})| / |Z(H_{sat})| \quad (1)$$

where $Z(H_{dc})$ is the impedance measured in the presence of the dc magnetic field H_{dc} and $Z(H_{sat})$ is the impedance measured at the saturation limit when the magnetization does not change any longer with the applied field.

2. The external dc magnetic field H_{dc} should be on the order of a few Oersteds only (see Table I on magnetic units and quantities).
3. The frequency range is on the order of MHz or tens of MHz (excluding any effect based on Ferromagnetic Resonance (FMR) where the frequencies are typically in the GHz range [5]). In many materials this means that the skin depth δ_s (typically microns at these frequencies) is larger than the thickness of the material (typically a fraction of a micron). When the frequency is in the GHz, δ_s is generally very small with respect to the thickness. It should be stressed that in ordinary metals, the skin depth does not depend on permeability, whereas in magnetic materials, the behavior of the permeability on geometry (see for instance section IV), temperature, stress, composition and so on, is reflected in the skin depth. In addition, permeability might be changed by post-processing the material after growth with annealing under presence or absence of magnetic field or mechanical stress...

GMI is a *classical phenomenon* that can be explained thoroughly on the basis of usual electromagnetic concepts [6, 7, 8] in sharp contrast with Giant Magnetoresistance (GMR) effect where

resistance is changed by a magnetic field. GMR requires Quantum Mechanical concepts based on the spin of the carriers and their interactions with the magnetization of the magnetic material. Several general conditions must be satisfied by any material in order to show a GMI.

1. The material should be magnetically soft. That is, it should be easily magnetised or in other words must have a relatively narrow hysteresis curve implying, in general, small losses in the course of the magnetization cycle.
2. The material should have a well defined anisotropy axis. That means there must be a direction along which the magnetization of the material lies on the average (easy axis). However the value of the anisotropy field H_k (see Fig. II) should be relatively small (on the order of a few Oersteds). The typical ratio of H_k to H_c must be about 20. That insures observation of large magnetoimpedance effects, typically.
3. The coercive field H_c must be small (fraction of an Oersted) and the hysteresis loop thin and narrow. Since H_c and the shape of the hysteresis loop change (see Fig. II) with the angle the magnetic field makes with the easy axis (or Anisotropy axis) of the material, these are taken at the reference point when the field is along the easy axis.
4. The ac current $I = I_0 e^{j\omega t}$, injected in the material, should be perpendicular to the easy axis (or anisotropy direction) and the magnetic field it creates H_{ac} should be small with respect to H_k (See Table I on magnetic units and quantities).
5. The material must have a small resistivity ($\leq 100 \mu\Omega.cm$) since it carries the ac current. This is important, since many magnetic materials have large resistivities. Amorphous metals are interesting in that respect since, typically, their resistivities at room temperature are in the $100 \mu\Omega.cm$ range.
6. The material should have a large saturation magnetization M_s in order to boost the interaction with the external magnetic field.
7. Above arguments are equivalent to a very large permeability at zero frequency (the ratio M_s/H_k gives a rough indication for this value). This means several 1000's (see Table II).
8. The material should have a small magnetostriction (MS). This means, mechanical effects caused by application of a magnetic field should be small. Mechanical stress due to MS

alters the soft properties of the material by acting as an effective anisotropy. This alters the direction of the anisotropy, displacing it from the transverse case and thereby reducing the value of the MI. Typical case materials are displayed along with their MS coefficient in Table II.

The general theory of the MI effect is widely available in classic textbooks [9] (for a long cylinder) and it has been shown experimentally that a large MI often occurs at frequencies of a few MHz. Changing the dc biasing field H_{dc} , the maximum $|Z|$ can be as large as a few times the value of R_{dc} the dc resistance. At low frequency $|Z|$ has a peak around $H_{dc} \sim 0$ and as the frequency increases, the peak moves toward $H_{dc} \sim \pm H_k$ where H_k is the anisotropy field. Therefore, $|Z|$ as a function of H_{dc} possesses a single or a double peak as the frequency increases (Fig. III). When the direction of the anisotropy field is well defined the peaks are sharp.

The behavior of $|Z|$ versus H_{dc} follows very closely the behavior of the real part of the transverse permeability versus H_{dc} as we will show in later sections on wires and ribbons. Therefore it is very important to develop an understanding for the processes controlling the permeability.

Material permeability depends on sample geometry, nature of exciting field, temperature, frequency, stress distribution in the material as well as internal configuration of the magnetization that might be altered by processing or frequency. For instance, some materials should be annealed under the presence of a magnetic field or a mechanical stress in order to favor some direction for the magnetization or to release the stress contained in them.

Regarding frequency, when it is large enough ($> 1\text{MHz}$ is sufficient in many materials) Domain Wall Displacements (DWD) are considerably reduced by eddy-currents and therefore magnetization varies by rotation or switching as if in a single domain (see Fig. II). As a consequence, the rotational motion of the magnetization controls the behaviour of the permeability, through the skin depth.

Considering a as a typical thickness (in the case of films/ribbons) or radius (in the case of wires or microwires), frequencies in the tens of MHz, lead to $\delta_s > a$ for the observation of GMI. This condition depends strongly on geometry. For instance, $\delta_s > a$ in 2D structures like films is satisfied at much higher frequencies (GHz) than in 1D structures like wires. This is simply

due to the optimal circular shape of wires that contains in an optimal fashion the flux while, simultaneously, carrying the ac current.

In terms of GMI performance, multilayered films (such as F/M/F where F is a ferromagnet and M is metallic non magnetic material) are preferred with respect to single layered films since they allow to inject the ac electric current in the metallic layer and sense the magnetic flux in neighbouring or sandwiching magnetic layers. These can be in direct contact with the metallic layer or separated from it by an insulator or a semiconductor. Flux closure, that increases GMI, occurs when the width of the film (transverse with respect to the ac current) is large or that the metallic layer is entirely buried in the magnetic structure to trap the flux.

The progress of GMI is thrust towards the increase of the largest value of the ratio $r(H_{dc})$ and the sensitivity given by the derivative of the ratio with respect to the field (see Table III for some illustrative values).

This sensitivity is simply estimated by looking at the behaviour of the permeability μ'_t versus H_{dc} as the frequency is changed. We ought to have a large variation of μ'_t about $H_{dc} \sim 0$. This happens, in general, at low frequencies that is when $\delta_s > a$. At high frequencies, we will show in later sections that this sensitivity is either lost or one has to go to higher H_{dc} to observe it hampering the use of the effect in small magnetic field detection.

Applications of GMI range from tiny magnetic field detection and sensing (such as magnetic recording heads) to magnetic field shielding (to degauss Cathode Ray Tubes (CRT) monitors). The reason is that GMI materials, being soft, possess large permeabilities that are required in magnetic shielding.

This work is organised as follows: In section II, a general discussion on soft materials is presented; in section III, GMI in wires is described. In section IV, GMI in films and ribbons is discussed. Section V highlights potential applications of GMI effect in Electronic and Sensing devices while Section VI bears conclusions and perspectives of GMI.

II. SOFT FERROMAGNETIC MATERIALS FOR GMI

Soft ferromagnetic materials (SFM) used in GMI applications play a key role in power distribution, make possible the conversion between electrical and mechanical energy, underlie microwave communication, and provide both the transducers and the active storage material for data storage in information systems. The fingerprint of any magnetic material is its hysteresis loop (HL) whose characteristic shape stems from two essential properties of magnetic materials: Non-linearity and delay between input and output signals. Non-linearity is given by the shape of the loop whereas the delay is given by the width of the HL. The quantities associated with the HL are displayed in Fig. II. In general, magnetic materials being anisotropic their HL width varies with the angle the external magnetic field makes with some given direction. The easy axis direction is defined as the direction for which the HL width (or coercive field H_c) is largest.

The coercive field H_c represents the effort to demagnetise any magnetic material. For instance, hard magnetic materials exhibit large resistance to demagnetization and are therefore used in materials requiring permanent magnets whereas SFM are used in devices demanding little effort to demagnetise or remagnetise. Hard magnets are used as permanent magnets for many electrical applications. Some rare-earth alloys based on SmCo_5 and $\text{Sm}(\text{Co}, \text{Cu})_{7.5}$ are used for small motors and other applications requiring an extremely high energy-product magnetic materials. Fe-Cr-Co alloys are used in telephone receivers and Nd-Fe-B is used for automotive starting motor.

In contrast, SFM possess a narrower loop than hard materials and the area within the hysteresis curve is small. This keeps the energy losses small, during each magnetic cycle, in devices based on these materials.

In order to qualify the different requirements for read heads and storage media in magnetic recording, an area belonging to the application portfolio of SFM (besides sensing and shielding), Table IV displays the desired characteristics.

SFM have high permeability (i.e. easily magnetized) with a low coercivity (i.e. easily demagnetized). Examples of soft ferromagnetic materials include Fe alloys (with 3 to 4% Si) used in motors and power transformers and generators. Ni alloys (with 20 to 50% Fe) used

primarily for high-sensitivity communications equipment. This illustrates the versatility of SFM applications that range from mechanical to electrical and from power to communications systems.

SFM exhibit magnetic properties only when they are subject to a magnetizing force such as the magnetic field created when current is passed through the wire surrounding a soft magnetic core. They are generally associated with electrical circuits where they are used to amplify the flux generated by the electric currents. These materials can be used in ac as well as dc electrical circuits.

Several types of SFM exist:

1. Soft mono and polycrystalline ferrites
2. Powder composite magnetic materials
3. Rapidly quenched ferromagnetic materials
4. Amorphous magnetic materials
5. Nanocrystalline magnetic materials

The soft ferromagnetic behavior in these materials arises from a spatial averaging of the magnetic anisotropy of clusters of randomly oriented small particles (typically < fraction of a micron). In some cases, the MS of these materials is also reduced to near zero.

Metallic glasses obtained by rapid quench (e.g. splat-cooling) are magnetically very soft. This property is used in multilayered metallic glass power transformer cores.

Amorphous magnetic alloys such as CoP first reported in 1965 and splat-cooled materials with attractive soft ferromagnetic properties are based either on 3d transition metals (T) or on 4f rare-earth metals (R). In the first case, the alloy can be stabilized in the amorphous state with the use of glass forming elements such as boron, phosphorus and silicon: Examples include $\text{Fe}_{80} \text{B}_{20}$, $\text{Fe}_{40} \text{Ni}_{40} \text{P}_{14} \text{B}_6$, and $\text{Co}_{74} \text{Fe}_5 \text{B}_{18} \text{Si}_3$ ($\text{T}_x \text{M}_{1-x}$, with $15 < x < 30$ at %, approximately). The transition metals of late order (TL where TL=Fe, Co, Ni) can be stabilized in the amorphous state by alloying with early order transition metals (TE) of 4d or 5d type (TE= Zr, Nb, Hf): some examples are $\text{Co}_{90} \text{Zr}_{10}$, $\text{Fe}_{84} \text{Nb}_{12} \text{B}_4$, and $\text{Co}_{82} \text{Nb}_{14} \text{B}_4$ ($\text{TE}_{1-x} \text{TL}_x$, where x is roughly $5 < x < 15$ at %).

Nanocrystalline soft magnetic materials are derived from crystallizing amorphous ribbons of a specific composition such as the (Fe, B) based alloy family. This class of materials is characterized

by 10-25 nm sized grains of a body-centered-cubic (Fe, X) phase consuming 70-80% of the total volume, homogeneously dispersed in an amorphous matrix.

Two families of alloys show the best performance characteristics and have emerged as the best candidates to major SFM applications: Fe-Cu-Nb-B-Si (the "Finemet" family, see Table III) and Fe-Zr-(Cu)-B-(Si) (the "Nanoperm" family). The Finemet family is characterized by an optimum grain size of about 15 nm, exhibits good properties at high frequencies and is comparable to some of the best (and relatively costly) Co based amorphous materials. On the other hand, the grain sizes consistent with optimum performance are larger, around about 25 nm, in the Nanoperm family. The distinguishing feature of the Nanoperm family of alloys is the very low energy loss exhibited at low frequencies (60 Hz), offering the potential for application in electrical power distribution transformers.

A typical amorphous alloy with a small MS coefficient λ_s , is $\text{Co}_{70.4} \text{Fe}_{4.6} \text{Si}_{15} \text{B}_{10}$. It is obtained by alloying FeSiB that has a positive $\lambda_s = 25 \cdot 10^{-6}$ with CoSiB that has a negative $\lambda_s = -3 \cdot 10^{-6}$ coefficient. Some materials that result from this alloying can reach a very small value of λ_s . For instance, $(\text{Co}_{0.8} \text{Fe}_{0.06})_{72.5} \text{Si}_{12.5} \text{B}_{15}$ has $\lambda_s \sim -10^{-7}$ that can be considered as zero since typical values of λ_s are units or tens of 10^{-6} . This was obtained by varying systematically the concentration x in the compound $(\text{Co}_{1-x} \text{Fe}_x)_{72.5} \text{Si}_{12.5} \text{B}_{15}$. Starting with $x = 0$ the MS coefficient $\lambda_s = -3.0 \cdot 10^{-6}$ decreases steadily to a near zero value $\lambda_s = -10^{-7}$ for $x = 0.06$. Let us indicate, at this point, that a commercial product exists called Vitrovac 6025 with the composition $\text{Co}_{66} \text{Fe}_4 \text{Mo}_2 \text{Si}_{16} \text{B}_{12}$ that exhibits a value [10] of $\lambda_s = -1.4 \cdot 10^{-7}$.

A small negative value of λ_s is exploited in wires, as discussed in the next section, produces a magnetization profile that is circular in a plane perpendicular to the wire axis whereas a positive λ_s produces a radial magnetization profile.

III. GMI IN WIRES

The search for GMI in soft magnetic wires and microwires is a topic of interest related to possible applications as tiny field sensors.

At low frequencies (weak skin effect or large skin depth), the first order expansion term of the impedance $Z = R(\omega) + jX(\omega)$ versus frequency is responsible for the voltage field dependence. This term is represented by an inductance, which is proportional to the transverse permeability. When the skin effect is strong, the total impedance including resistance R and reactance X is field dependent through the penetration depth.

The general theory of the MI effect in a long cylinder is widely available in classic textbooks [9] and it has been shown experimentally that a large MI often occurs at frequencies of a few MHz. Changing the dc biasing field H_{dc} , the maximum $|Z|$ can be as large as a few times the value of R_{dc} for amorphous wires. Following Beach et al. [4] the behaviour of the permeability can be understood on the basis of a simple phenomenological model based on a single relaxation time τ for the magnetization that yields for the permeability:

$$\mu_t(\omega, H_{dc}) = \mu'_t + j\mu''_t; \quad \mu'_t = 1 + \frac{4\pi\chi_0(H_{dc})}{1 + \omega^2\tau^2}, \quad \mu''_t = \frac{4\pi\chi_0(H_{dc})\omega\tau}{1 + \omega^2\tau^2} \quad (2)$$

The behaviour of μ'_t depicted in Fig. IV indicates that the strongest variation of μ'_t with H_{dc} happens at low frequencies as required for a sensitive sensor whereas the variation gets totally smeared out at large frequencies. It also illustrates the existence of a finite frequency range for the GMI effect as already observed in Fig. I. The range is determined by the inverse time $1/\tau$ that controls relaxation processes of the transverse magnetization.

While GMR is usually attributed to the differential scattering of conducting electrons whose spins make particular angles with the local magnetization of different scattering centers, it was believed, like GMR, this effect also resulted from the electron scattering by ac current-induced domain wall oscillations. Many different models exist for the description of permeability of metallic samples. Such models start with a uniform dc permeability throughout the sample, and then consider a class of domain structures with a magnetization process of DWD or domain magnetization rotations (DMR). In the case of ac impedance, standard quantitative models are used without considering domain structures. Therefore, some current explanations of MI have to be made based on usual considerations with some additional modifications to include concepts of DWD, DMR, ferromagnetic resonance, and magnetic relaxation. For a straight wire of radius a , conductivity σ and permeability μ (see Fig. V) the expression for impedance is given by [9]:

$$\frac{Z}{R_{dc}} = \frac{R + jX}{R_{dc}} = \frac{ka J_0(ka)}{2 J_1(ka)} \quad (3)$$

where J_i is the i -th order Bessel function and $k = (1 + j)/\delta_s$ where the skin depth is given by $\delta_s = \frac{c}{\sqrt{2\pi\omega\sigma\mu}}$. c is the speed of light and σ the conductivity.

Since the ac current is applied along the wire axis perpendicularly to the anisotropy (Fig. V), it is again the transverse permeability μ that is considered here. In order to show that the behavior of Z is dictated by the permeability, let us consider firstly the low frequency case, i.e. $ka \ll 1$. Expanding the Bessel functions, yields:

$$\frac{Z}{R_{dc}} = 1 + \frac{1}{48}\left(\frac{a}{\delta_s}\right)^4 - j\frac{1}{4}\left(\frac{a}{\delta_s}\right)^2 \quad (4)$$

In the opposite high frequency case ($\delta_s \ll a$ or $ka \gg 1$), taking $a \sim 1$ mm whereas $\delta_s \sim 1\mu$ m, we can expand the Bessel function to obtain:

$$\frac{Z}{R_{dc}} = (1 + j)\frac{a}{2\delta_s} \quad (5)$$

This indicates that $\frac{Z}{R_{dc}}$ could reach a value of several 1000's at high frequencies. The same result is obtained in the case of microwires by rescaling all lengths (since we have, in this case, $a \sim 1\mu$ m). It should be pointed out that since the ac current is along the wire axis, the magnetic field produced is circular along or against the rotational magnetization profile (see Fig. V). Note that at the frequencies of interest (> 1 MHz), where we have the largest sensitivity to H_{dc} , eddy-currents heavily damp DWD.

In wires made of materials having a small negative λ_s , the magnetization and anisotropy field H_k run in a circular fashion in a plane transverse to the ac current as illustrated in Fig. V. The dc field H_{dc} acts to realign the magnetization along its direction, decreasing therefore the transverse permeability. Therefore, a positive λ_s cannot be used for GMI since the magnetization profile is rather radial.

The skin depth dependent classical formula does not account for the presence of domain walls that can alter the scattering of the carriers. Panina et al. [1] and Chen et al. [11] accounted for domain wall scattering and showed that the latter is efficient when the inter-domain distance λ (see Fig. V) to the wire radius a ratio $\lambda/a \leq 0.1$ for frequencies ~ 1 MHz or greater. Introducing a parameter $\theta = a\sqrt{\sigma\mu\omega}$, they argue that a change of MI by a factor of 10 (assuming a change of θ^2 by a factor between 7 and 700) yields a change of μ/μ_0 by a factor of 100 to 10,000. Using a resistivity $\rho = 1/\sigma = 125 \mu\Omega.cm$ and $2a=0.124$ mm, the frequency $f \sim 3.1$ MHz yields a factor

of 4 to 10 change in $|Z|$. Chen et al. [11] proved also that the classical limit is recovered when $\lambda/a \leq 0.01$. The interpretation of a single or a double peak in the MI versus H_{dc} is interpreted as resulting from scattering by DMR. The scattering increases as H_{dc} gets closer to the anisotropy field H_k and then decreases after reaching its maximum for $H_{dc} \sim \pm H_k$. Wires with very small anisotropy possess a single peak since the scattering maximum occurs at $H_{dc} \sim 0$. Frequency effects produce the same result as seen in Fig. III.

In the case of GMI effect in coated tubes such as the electroplated FeNi, FeNiCo, and CoP microwires, Kurlyandskaya et al. [12] found a huge enhancement factor approaching 800% in Fe₂₀Co₆Ni₇₄ layers (1 μ m-thick) electroplated onto CuBe nonmagnetic microwire (100 μ m diameter) at a frequency of 1.5 MHz. That shows the way for producing the largest GMI in these systems.

IV. GMI IN RIBBONS AND THIN FILMS

Sputtered or otherwise produced films or ribbons possess several advantages with respect to wires due to the possibilities of size reduction and increase of efficiency. Nevertheless, oblong or elongated ribbon or thin film geometries are preferred in order to emulate the wire case where the largest GMI ratios were obtained.

Since the main ingredients of GMI are a metal that carries an ac current and a nearby magnetic material that must sense strongly the flux, 2D materials or multilayers offer more flexibility than wires and experimentally, several excitation configuration become possible when we are dealing with a ribbon or a film.

The general MI measurement configuration (longitudinal, perpendicular, transverse) in ribbons and films is shown in Fig. VI. In films and ribbons, the domain wall configuration is similar to what goes on in wires in the sense domain walls are transverse with respect to the ac current. In Fig. VII neighbouring domains have magnetizations pointing in different directions and the magneto-impedance effect result from averaging over transverse domains like in the wire case.

When a probe current $I_0 e^{j\omega t}$ is applied to a film of thickness $2a$, the impedance is written as:

$$\frac{Z}{R_{dc}} = jka \coth(jka), \quad (6)$$

where R_{dc} is the dc resistance of the film and $k = (1 + j)/\delta_s$ with δ_s the skin depth given by, as before, $\delta_s = \frac{c}{\sqrt{2\pi\omega\sigma\mu}}$. Since the current is applied (in the ribbon case) along the ribbon axis, again the transverse permeability is considered. As in the wire case, it is possible to expand $\frac{Z}{R_{dc}}$ at low (or $ka \ll 1$) and high frequencies (or $ka \gg 1$) and show that μ_t controls its behavior with H_{dc} . At low frequencies ($ka \ll 1$), we get:

$$\frac{Z}{R_{dc}} = 1 - \frac{2j}{3} \left(\frac{a}{\delta_s}\right)^2 \quad (7)$$

whereas, at high frequencies ($ka \gg 1$):

$$\frac{Z}{R_{dc}} = 1 - j \frac{a}{\delta_s} \quad (8)$$

The domain wall configuration (see Fig. VII) permits to estimate the permeability in the case of weak anisotropy field (H_k small but finite). It should be stressed that domains, H_k and permeability are all transverse. When H_{dc} is longitudinal, it plays the role of a hard axis field since it is acting on the magnetization, to rotate it, hence decreasing the transverse permeability, similarly like in wires.

In order to increase the MI response, multilayers are preferred to single layered films/ribbons. If a sandwiched metallic layer carries the ac current that creates the flux in the neighbouring magnetic layers, the MI effect is considerably enhanced (Table III). Moreover, when the width $2b$ is large (Fig. VII) the ac flux loop is closed and stray magnetic fields small [13].

Multilayers of Permalloy ($\text{Ni}_{81}\text{Fe}_{19}$ denoted as Py) and Ag of the type $[\text{Py}(x \text{ \AA})/\text{Ag}(y \text{ \AA})]_n$ with thickness $x = 107 \text{ \AA}$ and 88 \AA , $y = 7 \text{ \AA}$ and 24 \AA and the number of layers $n=15$ and 100 were grown by Sommer et al. [14] with magnetron sputtering techniques. The case $n=100$ displayed a GMI effect of the order of 5 to 25 %. The thickness of the Py layer has a strong effect on the coercive field and consequently on the softness of the material. The coercive field H_c varies from 0.85 Oersted for $x=88 \text{ \AA}$ to reach 13.6 Oersted for $x=5000 \text{ \AA}$. As the Ag thickness varied from 7 to 24 \AA the MI effect changed from single peak to double peak structure in a fashion akin to the effect of frequency. Sommer and Chien [15] showed also that in the ribbon case, a double or a

single peak structure in the MI results from the direction of the applied magnetic field H_{dc} . When it is longitudinal (along the ribbon axis, see Fig. VII) a double peak at $H_{dc} \sim \pm H_k$ is observed, but when it is transverse the demagnetization factor perpendicular to the ribbon axis becomes important. That is responsible of an apparent *longitudinal* permeability that gives birth to a single peak MI. The ribbon MI is similar to the wire case, however MI in single layer films remains small and it is still an open problem to find ways to increase it dramatically like in coated microwires. Nevertheless, when multilayers are used (see Table III) the GMI ratio may attain 700%. This enhancement is due to the electrical insulation of the metallic layer carrying the ac current by sandwiching it with SiO_2 layers, the outer magnetic layers embodying the ac inductance created by the current.

V. APPLICATIONS OF GMI IN ELECTRONICS AND SENSING

Since GMI uses soft magnetic materials possessing a large permeability, the first immediate application is in devices related to magnetic shielding since it requires the soft properties of the material. A host of other applications involves the GMI per se.

The first of these applications are the detection of very small magnetic fields. In order to have a general idea of the scale of current magnetic Fields Table V displays some orders of magnitude of natural and artificial fields.

Detection of magnetic field is also important and magnetic field sensors (see Hauser et al. [16]) are broadly classified in three categories (see Table VI):

1. Medium to large field detection by Hall and magnetoresistive devices.
2. Small to medium magnetic field detection by magnetoimpedance and Flux Gate sensors.
3. Very small to small magnetic field detection by SQUID's (Superconducting QUantum Interference Devices).

The possible devices are recording read heads, magnetic guidance devices in vehicles, boats and planes (with or without GPS, i.e. Global Positioning System), brain imaging (magnetoencephalogram or MEG devices) and heart mapping (magneto-cardiogram or MCG devices) etc...

The detection of the Earth magnetic field has a host of applications for instance in Petroleum or minerals exploration or in shielding used for Degaussing of High performance CRT monitors...

The general features required for sensors are not only high sensitivity, flexibility, large bandwidth and low cost but linearity is also a desired feature. In order to increase the sensitivity of GMI devices with respect to the dc magnetic field, devices were developed [17] possessing non-symmetric variation of the MI with respect to H_{dc} . The materials used are field annealed Co-based amorphous ribbons ($\text{Co}_{66}\text{Fe}_4\text{NiB}_{14}\text{Si}_{15}$) (see Table III). The asymmetry of the MI profile allows a very sensitive detection of the magnetic field specially around $H \sim 0$ and when the asymmetry of the profile is so sharp that it becomes step-like, we have a so-called "GMI valve" based device. In these devices, the sensitivity might be enhanced to reach 1000%/Oe (compare with values in Table III). Asymmetry may also be induced by torsional stress such as in wires of $\text{Fe}_{77.5}\text{Si}_{7.5}\text{B}_{15}$ [18]. Altering the GMI response with mechanical stress paves the way toward the development of strain sensors that can be used in several areas of engineering and science.

VI. CONCLUSION

Good candidates for GMI are amorphous Cobalt rich ribbons, wires, glass covered microwires and multilayers made of a metallic layer sandwiched between ferromagnetic materials (with or without intermediate insulating layers).

Zero-field annealing or annealing under a magnetic field or with the application of some mechanical stress favors orienting the magnetization along a desired direction. In order to get a fast reduction of the transverse permeability (see Fig. IV) under the application of an external field H_{dc} , there must be an optimal distribution of the magnetization around the desired direction [1] and that can be obtained with suitable growth or annealing conditions. Reduction of the stress contained into the as-grown materials by sputtering or quenching can also be obtained with annealing.

The current activity in GMI studies is oriented toward the development of devices using a built-in magnetic field rather than an applied external field. This is reminiscent of the p-n, Schottky, heterojunctions etc... where the built-in field is electrical.

The discovery of magnetic bias produced a revolution in magnetism because of the many potential applications in storage, sensing, spintronics... Nevertheless, there are other ways to produce built-in magnetic fields. For instance Ueno et al. [19] produced such an internal field by

superposing two sputtered films of $\text{Co}_{72} \text{Fe}_8 \text{B}_{20}$ with crossed anisotropy axes, i.e. with the anisotropy axis of the bottom layer making angles of opposite sign with some common direction. While GMI in wires and ribbons is steadily progressing, the case of single layered films is still lagging behind in favor of multilayered films. Ways must be developed in order to increase the sensitivity of single or multilayered structures in order to reach the level observed in wires and microwires. The range of applications will substantially explode once GMI in thin films will be competitive with wires and ribbons.

Acknowledgement

The authors wish to acknowledge correspondance with P. Ripka and his kind providing of re(pre)prints of his work as well as friendly discussions with A. Fessant regarding characterisation and impedance measurements.

-
- [1] L. V. Panina and K. Mohri, *Appl. Phys. Lett.* 65, 1189 (1994).
 - [2] R. S. Beach and A. E. Berkowitz, *Appl. Phys. Lett.* 64, 3652 (1994).
 - [3] F. L. Machado, B. L. da Silva, S. M. Rezende and C. S. Martins, *J. Appl. Phys.* 75, 6563 (1994).
 - [4] R. S. Beach and A. E. Berkowitz, *J. Appl. Phys.* 76, 6209 (1994).
 - [5] M. R. Britel, D. Menard, L. G. Melo, P. Ciureanu, A. Yelon, R. W. Cochrane, M. Rouahbi and B. Cornut, *Appl. Phys. Lett.* 77, 2737 (2000).
 - [6] D. Atkinson and P. T. Squire, *J. Appl. Phys.* 83, 6569 (1998).
 - [7] M. Knobel and K. R. Pirota, *JMMM* 242-245, 33 (2002).
 - [8] R. Valenzuela, M. Knobel, M. Vazquez and A. Hernando, *J. Appl. Phys.* 78, 5189 (1995).
 - [9] L. D. Landau and E. M. Lifshitz, *Electrodynamics of Continuous Media*, Pergamon, Oxford, p.195 (1975).
 - [10] N. Murillo, J. Gonzalez, J. M. Blanco, R. Valenzuela, J. M. Gonzalez and J. Echebarria, *J. Appl. Phys.* 81, 5683 (1997).
 - [11] D-X Chen, J.L. Munoz, A. Hernando and M. Vazquez, *Phys. Rev.* 57, 10699 (1998).
 - [12] G. V. Kurlyandskaya, J. M. Barandiaran, J. L. Munoz, J. Gutierrez, D. Garcia, M. Vazquez, and V. O. Vaskovskiy, *J. Appl. Phys.* 87, 4822 (2000).

- [13] A. Paton, *J. Appl. Phys.* 42, 5868 (1971).
- [14] R. L. Sommer, A. Gündel and C. L. Chien, *J. Appl. Phys.* 86, 1057 (1999).
- [15] R. L. Sommer and C. L. Chien, *Appl. Phys. Lett.* 67, 3346 (1995).
- [16] H. Hauser, L. Kraus and P. Ripka, *IEEE Inst. and Meas. Mag.* 28 (2001).
- [17] C.G. Kim, K.J. Jang, D.Y. Kim and S.S. Yoon: *Appl. Phys. Lett.* 75, 2114 (1999).
- [18] G.H. Ryu, S.C. Yu, C. G. Kim, I.H. Nahm and S.S. Yoon, *J. Appl. Phys.* 87, 4828 (2000).
- [19] K. Ueno, H. Hiramoto, K. Mohri, T. Uchiyama and L. V. Panina, *IEEE Trans. Mag.* 36, 3448 (2000).

FIGURES AND TABLES

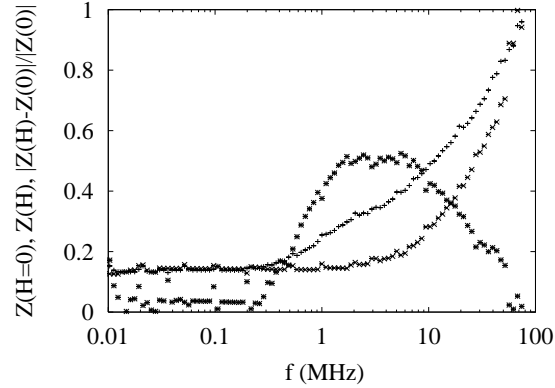


FIG. I: Normalised impedance $Z(H=0)$ and $Z(H)$ versus frequency for amorphous $\text{Fe}_{4.3} \text{Co}_{68.2} \text{Si}_{12.5} \text{B}_{15}$ wire (30 micron diameter) with $H=10$ Oe. The upper monotonous curve (+) is $Z(H = 0)$, the lower monotonous curve (x) is $Z(H)$ and the bumpy curve (*) is the ratio $|Z(H) - Z(H = 0)|/|Z(0)|$. The largest ratio reaches 60 %. Note the finite frequency range where the large variation is observed. The figure is adapted from Panina et al. [1].

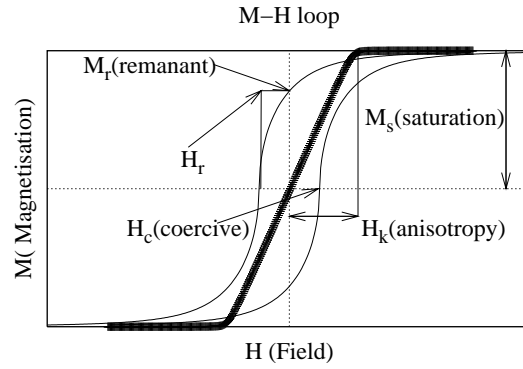


FIG. II: Single domain hysteresis loop obtained for an arbitrary angle, α , between the magnetic field and the anisotropy axis. Associated quantities such as coercive field H_c , remanent magnetization M_r and field H_r (given by the intersection of the tangent to the loop at $-H_c$ and the M_r horizontal line) are shown. The thick line is the hysteresis loop when the field is along the hard axis ($\alpha=90$ degrees, in this case) and H_k is the field value at the slope break. Quantities such as H_c , M_r and H_r depend on α .

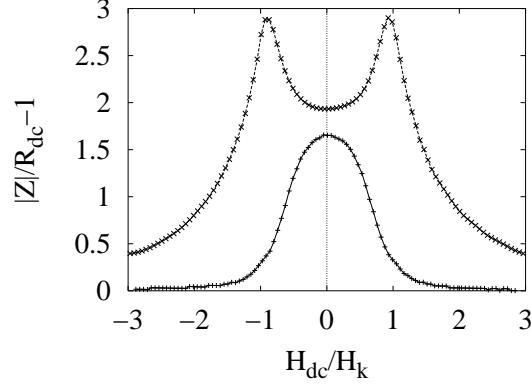


FIG. III: Variation of normalised impedance $|Z|/R_{dc}$ versus magnetic field H_{dc} at fixed low (single peak) and high frequency (double peak). As the frequency increases, the peak shifts toward the anisotropy field $\pm H_k$. That is why at low frequency a single peak is observed. The rounding of the peaks is due to a distribution of the anisotropy field direction.

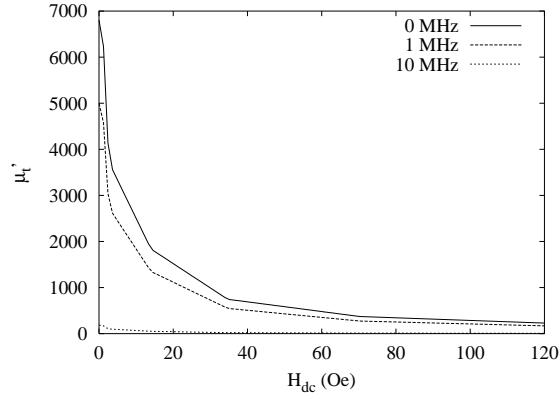


FIG. IV: Variation of the transverse permeability versus magnetic field H_{dc} . The physical quantities used are the same of Beach et al. [2] such as the experimentally determined function $\chi_0(H_{dc})$ and the inverse relaxation time $\frac{1}{\tau} = 10.45$ MHz. The latter determines the range of variation of interest for the permeability.

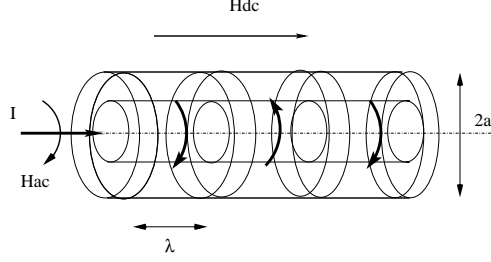


FIG. V: Bamboo-like domain wall structure in a cylindrical wire with magnetization profiles counter-rotating about a central core where the ac current I circulates. It is the small negative value of MS λ_s that induces a circumferential residual anisotropy through the inverse magnetostriction effect [1] producing the circular magnetization profiles. The resulting circular anisotropy axis (easy axis), along the magnetization is perpendicular to the direction of the ac current. Therefore, the dc field H_{dc} plays the role of a hard axis that damps magnetization and consequently decreases the permeability. A positive λ_s results in a radial magnetization profile that cannot be exploited in GMI applications.

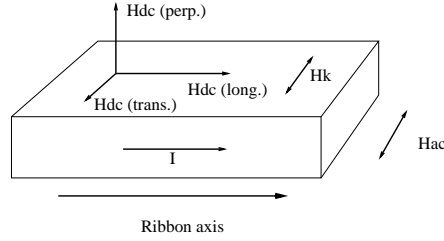


FIG. VI: General magnetoimpedance measurement setup in an elongated ribbon. The static field \mathbf{H}_{dc} might be longitudinal, transverse or perpendicular to the ac current $I = I_0 e^{j\omega t}$ that creates the alternating transverse \mathbf{H}_{ac} . H_k is the anisotropy field, transverse to the ac current direction. When \mathbf{H}_{dc} is longitudinal, it plays the role of a hard axis field like in wires that decreases the transverse permeability.

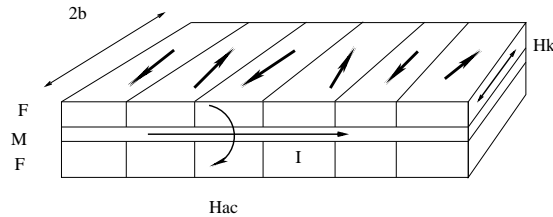


FIG. VII: Domain wall configuration in a multilayered structure. The magnetization direction is shown in every domain. The ac current flows in the sandwiched metallic layer, producing an ac flux in the surrounding magnetic layers.

Physical Quantity	SI	CGS
Bohr magneton μ_B	$0.927 \cdot 10^{-23} \text{ A}\cdot\text{m}^2$	$0.927 \cdot 10^{-20} \text{ emu}^a$
Vacuum permeability μ_0	$4\pi \cdot 10^{-7} \text{ V}\cdot\text{s}/\text{A}\cdot\text{m}$	1
Field Strength H	A/m	$4\pi \cdot 10^{-3} \text{ Oe}$
Example	80 A/m	$\sim 10 \text{ Oe}$
Polarisation or magnetization with saturation value M_s	$\mu_0 M_s$	$4\pi M_s$
Example M_s^b	1 A/m	$4\pi \cdot 10^{-3} \text{ emu}/\text{cm}^3$
Induction B	$B = \mu_0(H + M)$	$B = H + 4\pi M$
Example	1 Tesla = $1 \text{ V}\cdot\text{s}/\text{m}^2$	10^4 G
Susceptibility	$M = \chi H$	$M = \chi H$
Example	$\chi = 4\pi$	$\chi = 1$
Energy density of magnetic Field	$BH/2$	$BH/8\pi$
Example	$1 \text{ J}/\text{m}^3$	$10 \text{ erg}/\text{cm}^3$
Energy of magnetic matter in an external field	$\mu_0 H dM$	$H dM$
Anisotropy constant K	$10^5 \text{ J}/\text{m}^3$	$10^6 \text{ erg}/\text{cm}^3$
Anisotropy Field	$H_K = 2 \frac{K}{\mu_0 M_s}$	$H_K = 2 \frac{K}{M_s}$
Example	$10^6 \text{ A}/\text{m}$	$4\pi \cdot 10^3 \text{ Oe}$
Exchange Field	$\frac{J}{\mu_B}$	$\frac{J}{\mu_B}$
Example	$10^9 \text{ A}/\text{m}$	$4\pi \cdot 10^6 \text{ Oe}$
Demagnetising field in a thin film	$-M_s$	$-4\pi M_s$
Energy density of Demagnetising field in thin film	$\mu_0 M_s^2 / 2$	$2\pi M_s^2$
Magnetostriction coefficient	$\pm \lambda_s \sim 10^{-6}$	$\pm \lambda_s \sim 10^{-6}$

^aalso expressed in erg/Oe

^bIt is also expressed in Gauss with 1Gauss= $1 \text{ emu}/\text{cm}^3$

TABLE I: Correspondance between magnetic Units in the SI and CGS unit systems. Note that magnetic field units are A/m and Oe and Induction's are Tesla and Gauss. In vacuum or non-magnetic materials in CGS values in Oe and Gauss are same.

Alloy	H_c (mOe)	μ_{max} at 50 Hz	magnetostriction ^a Coefficient
Fe ₈₀ B ₂₀	40	320, 000	$\lambda_s \sim 30. \times 10^{-6}$
Fe ₈₁ Si _{3.5} B _{13.5} C ₂	43.7	260, 000	
Fe ₄₀ Ni ₄₀ P ₁₄ B ₆	7.5	400, 000	$\lambda_s \sim 10. \times 10^{-6}$
Fe ₄₀ Ni ₃₈ Mo ₄ B ₁₈	12.5-50	200, 000	
Fe ₃₉ Ni ₃₉ Mo ₄ Si ₆ B ₁₂	12.5-50	200, 000	
Co ₅₈ Ni ₁₀ Fe ₅ (Si, B) ₂₇	10-12.5	200, 000	$\lambda_s \sim 0.1 \times 10^{-6}$
Co ₆₆ Fe ₄ (Mo, Si, B) ₃₀	2.5-5	300, 000	

^aIt is defined as $\lambda_s = \delta l/l$, the largest relative change in length due to application of a magnetic field

TABLE II: Examples of soft magnetic materials and their hierarchy according to λ_s . The main composition is successively based on Fe, NiFe and finally Co. A commercial compound, close to the last family, Vitrovac 6025 ® or Co₆₆ Fe₄ Mo₂ Si₁₆ B₁₂ has [10] $\lambda_s = -1.4 \cdot 10^{-7}$

Material	$\max(r(H_{dc}))^a$	$\max(dr(H_{dc})/dH_{dc})$ (% /Oe)	Frequency (MHz)
Amorphous microwire: Co _{68.15} Fe _{4.35} Si _{12.5} B ₁₅	56	58.4	0.9
Finemet wire ^b	125		4
Amorphous wire: Co _{68.15} Fe _{4.35} Si _{12.5} B ₁₅	220	1760	0.09
CoP multilayers electroplated on Cu wire	230		0.09
Mumetal ^c , stripe	310	20.8	0.6
Textured Fe-3% Si sheet	360		0.1
Amorphous ribbon: Co _{68.25} Fe _{4.5} Si _{12.25} B ₁₅	400		1
Ni ₈₀ Fe ₂₀ electroplated on non-magnetic CuBe microwire	530	384	5
Sandwich film: CoSiB/SiO ₂ /Cu/SiO ₂ /CoSiB	700	304	20
FeCoNi electroplated on non-magnetic CuBe microwire	800		1.5

$$^a r(H_{dc}) = 100 \times |Z(H_{dc}) - Z(H_{sat})| / |Z(H_{sat})|$$

^bFe-Cu-Nb-B-Si family

^c77% Ni, 16% Fe, 5% Cu, 2% Cr

TABLE III: Materials for GMI sensors: wires and films adapted from Hauser et al. [16]. The GMI ratio is given in the second column whereas the sensitivity with respect to the magnetic field is given by the largest value of the derivative of the ratio (third column).

HL quantity	Head core	Recording Media
M_s	Large	Moderate
M_r	Small	Large
H_c	Small	Large
$S = M_r/M_s$	Small ~ 0	~ 1
$S_c = \left(\frac{dM}{dH}\right)_{H=H_c}$	Large	
$S^* = 1 - \frac{(M_r/H_c)}{S_c}$		~ 1

TABLE IV: Requirements on read head and recording media from HL. The parameters S and S* are the remanant and the loop squareness respectively. S* represents the steepness of the HL at the coercive field, i.e. the slope of the HL at H_c is $S_c = \left(\frac{dM}{dH}\right)_{H=H_c} = \frac{M_r}{H_c(1-S^*)}$. In practice a fairly square HL has S, S* ~ 0.85 .

Magnetic induction ^a occurrence	Typical Range	Typical Range
Type of Induction	(in Gauss)	(in Tesla)
Biological		
Body or brain of man ^b , animals...	$10^{-10} - 10^{-5}$ Gauss	$10^{-14} - 10^{-9}$ Tesla ^c
Geological		
Inside Earth	10^{10} Gauss	10^6 Tesla
On the Earth surface	$10^{-4} - 1$ Gauss ^d	
Superconducting Coil	$> 25 \cdot 10^4$ Gauss	> 25 Teslas

^amagnetic field is expressed in Oe and induction in Gauss.

^bThe magnetic induction of the Human Brain is about 10^{-13} Tesla

^cHuman heart induction is around 10^{-10} Tesla

^dTransverse component of the Earth magnetic induction is 0.5 Gauss

TABLE V: Natural and artificial magnetic induction in various systems. Note that magnetic field unit is A/m and Oe and Induction is Tesla and Gauss. In vacuum or non-magnetic materials in CGS values in Oe and Gauss are same.

Sensor type	Magnetic induction typical range (in Gauss)	typical sensitivity (in Gauss)
Hall	$1 - 10^6$	10.
Magnetoresistance	$1 - 10^6$	1.
Magnetoimpedance	$10^{-6} - 1$	10^{-6}
Flux Gate	$10^{-6} - 1$	10^{-6}
SQUID	$10^{-9} - 10^{-6}$	10^{-10}

TABLE VI: Magnetic induction sensor types, range and typical sensitivity. Note that magnetic field unit is A/m and Oe and induction is Tesla and Gauss. In vacuum or non-magnetic materials, CGS values in Oe and Gauss are same.